Monthly Notices of the ROYAL ASTRONOMICAL SOCIETY

MNRAS **498,** 3215–3227 (2020) doi:10.1093/mnras/staa2556
Advance Access publication 2020 August 22

Gas accretion regulates the scatter of the mass–metallicity relation

Gabriella De Lucia [1]★, Lizhi Xie [2], Fabio Fontanot [1,3] and Michaela Hirschmann [4]

[1] *INAF – Astronomical Observatory of Trieste, via G.B. Tiepolo 11, I-34143 Trieste, Italy*
[2] *Tianjin Astrophysics Center, Tianjin Normal University, Binshuixidao 393, 300384 Tianjin, China*
[3] *IFPU – Institute for Fundamental Physics of the Universe, via Beirut 2, I-34151 Trieste, Italy*
[4] *DARK, Niels Bohr Institute, University of Copenhagen, Lyngbyvej 2, DK-2100 Copenhagen, Denmark*

Accepted 2020 August 18. Received 2020 August 15; in original form 2020 May 2

ABSTRACT

In this paper, we take advantage of the GAlaxy Evolution and Assembly (GAEA) semi-analytic model to analyse the origin of secondary dependencies in the local galaxy mass–gas metallicity relation. Our model reproduces quite well the trends observed in the local Universe as a function of galaxy star formation rate and different gas-mass phases. We show that the cold gas content (whose largest fraction is represented by the atomic gas phase) can be considered as the third parameter governing the scatter of the predicted mass–metallicity relation, in agreement with the most recent observational measurements. The trends can be explained with fluctuations of the gas accretion rates: a decrease of the gas supply leads to an increase of the gas metallicity due to star formation, while an increase of the available cold gas leads to a metallicity depletion. We demonstrate that the former process is responsible for offsets above the mass–metallicity relation, while the latter is responsible for deviations below the mass–metallicity relation. In low- and intermediate-mass galaxies, these negative offsets are primarily determined by late gas cooling dominated by material that has been previously ejected due to stellar feedback.

Key words: Galaxy: abundances – Galaxy: evolution – Galaxy: formation – galaxies: ISM.

1 INTRODUCTION

Our quest to understand the formation and evolution of galaxies often proceeds through the study of well-defined correlations between their physical properties. One of these relates the total galaxy stellar mass to the gaseous metallicity. The former quantity represents the integrated mass of gas that has been locked up in stars, while the latter reflects the recycling of gas and metals from stars and the exchanges of gas between the galaxy and its surroundings (inflows and outflows). First observations of a correlation between gas metallicity and galaxy luminosity (as a proxy for galaxy mass) date back to the 1970s (McClure & van den Bergh 1968; Lequeux et al. 1979), and have been followed by more detailed studies based on larger samples (e.g. Skillman, Kennicutt & Hodge 1989; Zaritsky, Kennicutt & Huchra 1994). The advent of large spectroscopic surveys, and the development of more sophisticated stellar population models have allowed major advances in our ability to measure galaxy physical properties. The benchmark on the subject has been provided by Tremonti et al. (2004), who used ∼53 000 galaxies from the Sloan Digital Sky Survey (SDSS) to demonstrate the existence of a very tight relation between the gas-phase metallicity and galaxy stellar mass. The shape and normalization of the relation depend on the metallicity calibration adopted (Kewley & Ellison 2008), which has to be taken into account carefully when interpreting e.g. the evolution of the relation to higher redshift or when comparing data from different studies. A tight correlation is found up to $z \sim 3.5$, i.e. the highest redshift where all main optical lines are still in the near-IR (e.g. Maiolino et al. 2008; Troncoso et al. 2014; Onodera et al. 2016; Sanders et al. 2020, just to cite a few).

Different explanations have been proposed for the origin of the mass–metallicity relation. The classical interpretation is based on selective losses of metals into the intergalactic medium by low-mass galaxies, due to galactic winds generated by the energy released by massive stars and supernovae (e.g. Larson 1974; Tremonti et al. 2004; Chisholm, Tremonti & Leitherer 2018). An alternative possibility is that the observed relation reflects different evolutionary stages of galaxies with different mass: High-mass galaxies evolve more rapidly at higher redshift than their lower mass counterparts, that still have to convert most of their gas into stars (e.g. Maiolino et al. 2008; Zahid, Kewley & Bresolin 2011). In addition, given the low star formation rates measured in low-mass galaxies, infall of pristine gas is a viable mechanism to dilute their interstellar medium (Köppen & Edmunds 1999; Dalcanton 2007). Finally, variations of the stellar initial mass function (IMF) could lead to systematic differences of the metal yields as a function of the galaxy stellar mass (Köppen, Weidner & Kroupa 2007). In reality, of course, all these effects are likely simultaneously present, so that a correct interpretation of the observed trends requires theoretical models that are fully embedded in a cosmological framework, and that include all the relevant physical processes.

The existence of a *secondary dependence* in the mass–metallicity relation was already studied in Tremonti et al. (2004). These authors found that the residuals from the best-fitting relation correlate with the local surface mass density measured within the fibre aperture and somewhat with colours, but not with the Hα equivalent width (see their fig. 7). Later studies, based on the same data sample (Lara-López et al. 2010; Mannucci et al. 2010), have identified a strong

★ E-mail: gabriella.delucia@inaf.it

dependence on the star formation rate, that has been framed in terms of a more general relation between galaxy stellar mass, gas-phase metallicity, and star formation rate. This three-dimensional relation can be explained in terms of a more fundamental relation with the gas content of galaxies (or gas fraction): Larger amounts of gas lead to increasing star formation rates and therefore to increasing values of the gaseous metallicity, while a decreasing metallicity is expected with dilution caused by larger amounts of newly accreted gas (e.g. Dayal, Ferrara & Dunlop 2013; Lilly et al. 2013). A strong correlation between gas fraction/gas content and metallicity, at fixed stellar mass, has indeed been observed in the local Universe (Hughes et al. 2013; Bothwell et al. 2016; Brown et al. 2018). These studies have shown that the correlation with gas content is significantly stronger than that with the star formation rate (either total or measured within a fibre), independently of the metallicity calibration adopted. While outflows can contribute to the scatter in the observed mass–metallicity relation, the observed trends suggest that it is primarily driven by fluctuations in accretion rates of (pristine) gas (see discussion in Brown et al. 2018). This picture is supported by models assuming 'equilibrium' solutions in which gas inflow is compensated by star formation and outflows (e.g. Davé, Finlator & Oppenheimer 2012; Lilly et al. 2013). This formalism is useful to understand the origin of the main trends and appears to be able to broadly capture, at least to first order, results from more complex theoretical models of galaxy formation. It is, however, not appropriate to characterize the contribution from different physical processes to the scatter in the observed scaling relations, and to fully account for the variety of galaxy evolutionary histories driven by structure formation.

Cosmological models of galaxy formation (both semi-analytic models and hydrodynamical simulations) have long had problems in reproducing well the shape of the observed mass–metallicity relation at $z = 0$ and, in particular, its evolution to higher redshift (see the discussion in Somerville & Davé 2015, and their fig. 6). More recent renditions of these theoretical models exhibit a significantly better agreement with data (Hirschmann, De Lucia & Fontanot 2016; De Rossi et al. 2017; Xie et al. 2017; Collacchioni et al. 2018; Torrey et al. 2019). In some cases, an analysis of the scatter of the mass–metallicity relation and its origin has been carried out. Yates, Kauffmann & Guo (2012) studied the dependence of the cold gas metallicity on star formation rate, in an earlier version of the semi-analytic model L-GALAXIES (in particular, they use the model published in Guo et al. 2011). They find a star formation rate dependence that is qualitatively similar to that observed, but their work focuses on the reversal of the dependence for low- and high-mass galaxies. More recently, Lagos et al. (2016) have used a principal component analysis to show that the atomic gas fraction, stellar mass, and star formation rate account for most of the variance in the galaxy population predicted by the EAGLE simulations. They argue that this 'Fundamental Plane' arises from the self-regulation of the star formation in galaxies. Torrey et al. (2019) analyse the evolution of the mass–metallicity relation within the IllustrisTNG simulation suite. They find a correlation between the scatter in the predicted relation and the galactic gas mass, that they argue can be explained as a competition between periods of gas-rich enrichment domination and periods of gas-poor, accretion domination. To date, no systematic comparison has been carried out between predictions of the most recent theoretical models and the accurate measurements available in the local Universe for trends as a function of *both* star formation rates and the different gas-phase components. In addition, a detailed quantification of the physical processes responsible for the predicted trends has not been published yet.

In this paper, we take advantage of a state-of-the-art semi-analytic model that includes an accurate treatment for the non-instantaneous recycling of metals, gas, and energy, as well as a treatment for the partition of the cold gas in atomic and molecular hydrogen, and analyse the origin of secondary dependencies in the mass–metallicity relation at $z = 0$. A brief overview of the model used in this work is given in Section 2. In Section 3, we present the basic predictions of our model and compare them with recent observational measurements. In Section 4, we analyse the contribution of different physical processes to the scatter of the mass–metallicity relation. Finally, in Section 5, we discuss our results and give our conclusions.

2 THE GALAXY FORMATION MODEL

In this work, we use an updated version of the GAlaxy Evolution and Assembly (GAEA) semi-analytic model (Hirschmann et al. 2016). GAEA descends from the model originally published in De Lucia & Blaizot (2007), but the treatment of various physical processes has been significantly updated since then. In particular, the GAEA version used in this study includes (i) a sophisticated scheme to account for the non-instantaneous recycling of gas, energy, and metals (De Lucia et al. 2014), which allows us to trace the evolution of individual metal abundances; (ii) a stellar feedback scheme that is partly based on hydrodynamical simulations, and that allows us to reproduce the evolution of the galaxy stellar mass function up to $z \sim 7$ and the cosmic star formation rate density up to $z \sim 10$ (Hirschmann et al. 2016; Fontanot, Hirschmann & De Lucia 2017); and (iii) a self-consistent treatment to partition the cold gas in its atomic and molecular hydrogen components (Xie et al. 2017), which will allow us to analyse explicitly the dependence of the mass–metallicity relation on different components of the cold gaseous phase. Specifically, we use here the parametrizations based on the empirical prescriptions by Blitz & Rosolowsky (2006) that, in the framework of our model, provide a good agreement with the scaling relations observed in the local Universe. We refer to the original papers mentioned above for full details on the modelling adopted for different physical processes. Briefly, we assume that infalling gas has primordial chemical composition and condenses at the centre of dark matter haloes, settling in a gaseous disc whose radius is estimated by tracing the angular momentum evolution of the gas (Xie et al. 2017). In the regions of highest gas densities, atomic gas can be efficiently converted in molecular hydrogen that represents, in our model, the fuel for star formation. The energy from supernovae explosions and massive stars drives efficient galactic scale winds that can eject significant amounts of gas and metals outside the parent dark matter haloes. The ejected gas can later be re-incorporated, on time-scales that are assumed to depend on halo mass (Hirschmann et al. 2016, and references therein). In our model, we always assume that metal flows occur proportionally to mass flows between different galactic components.

In previous work, we have shown that our reference GAEA model is able to reproduce a number of important observational constraints. Notably for this study, it is one of the few recently published theoretical models able to reproduce the observed correlation between galaxy stellar mass and gas metallicity, as well as its evolution as a function of redshift (Hirschmann et al. 2016; Xie et al. 2017), without assuming the chemical yield as a free parameter. It therefore represents an ideal tool to investigate the origin of secondary dependencies in such a correlation.

The model predictions presented in the following are based on merger trees extracted from the Millennium Simulation (Springel et al. 2005). The simulation follows 2160^3 dark matter particles in a

box of 500 Mpc h^{-1} on a side, and assumes cosmological parameters consistent with WMAP1 ($\Omega_\Lambda = 0.75$, $\Omega_m = 0.25$, $\Omega_b = 0.045$, $n = 1$, $\sigma_8 = 0.9$, and $H_0 = 73\,km\,s^{-1}\,Mpc^{-1}$). Recent measurements provide slightly different cosmological parameters (in particular, a larger value for Ω_m and a lower value for σ_8). As we have shown in previous work, however, these differences do not affect significantly model predictions once the parameters of the model have been retuned to reproduce a given set of observational measurements in the local Universe (Wang et al. 2008). Simulation data were stored in 64 outputs that are approximately logarithmically spaced in time between $z = 20$ and 1, and linearly spaced in time for $z < 1$. The differential equations governing the evolution of model galaxies are solved dividing the time interval between two subsequent snapshots in 20 equal sub-steps that, in our reference runs, correspond to a maximum of ∼18.8 Myr.

For the analysis presented below, we have used only about 6 per cent of the volume of the simulation, but we have verified that results do not vary significantly when considering a larger volume. The comparison with data presented in Section 3 is based on 20 per cent of the volume of the simulation.

3 SECONDARY CORRELATIONS IN THE (GAS) METALLICITY–GALAXY MASS RELATION

Fig. 1 shows the gas metallicity–stellar mass relation predicted by our model (coloured distribution and solid black lines), compared with different observational measurements. In particular, dashed lines show the 16th and 84th percentiles of the distribution measured by Tremonti et al. (2004) using SDSS spectra from DR2, and fitting simultaneously all most prominent emission lines. The empty triangles show a re-determination of the mass–metallicity relation by Kewley & Ellison (2008), based on spectra from DR4 with tighter limits on the redshift range ($0.04 < z < 0.1$). With this selection, the projected SDSS fibre covers more than 20 per cent of the total g-band light, and incompleteness at higher redshift is minimized. The empty triangles correspond to a metallicity calibration based on photoionization models (Kewley & Dopita 2002), which suffers of similar biases and uncertainties of the strong-line method used by Tremonti et al. (2004; see the discussion in Kewley & Ellison 2008 for details). Crosses with error bars show measurements by Bothwell et al. (2016), based on a sample of local galaxies with available measurements of both molecular and total gas mass. Specifically, the data come mainly from three surveys: COLD GASS (Saintonge et al. 2011), the Herschel Reference Survey (Boselli, Cortese & Boquien 2014), and ALLSMOG (Bothwell et al. 2014). Also for this sample, metallicity estimates are based on optical strong-line fluxes. Finally, open circles with error bars show measurements by Curti et al. (2020). These authors have re-analysed the SDSS data using a new metallicity calibration based on the T_e abundance scale (Curti et al. 2017). All observational measurements shown assume a Kroupa (2001) stellar IMF, which is very similar to the Chabrier (2003) IMF adopted in our reference model (in the case of Curti et al., the stellar mass measurements have been already rescaled to a Chabrier IMF). As mentioned in Section 1, the shape and normalization of the mass–metallicity relation depend significantly on the calibration adopted. It is well known, and this is clearly shown in Fig. 1, that there are large systematic offsets between estimates based on theoretical calibrations and electron temperature metallicities. The origin of these offsets remains unclear, but it is generally accepted that calibrations based on strong emission lines and photoionization models tend to overestimate the true metallicities, while methods based on the electron temperature can underestimate them (e.g. Kewley & Ellison 2008; Maiolino & Mannucci 2019, and references therein).

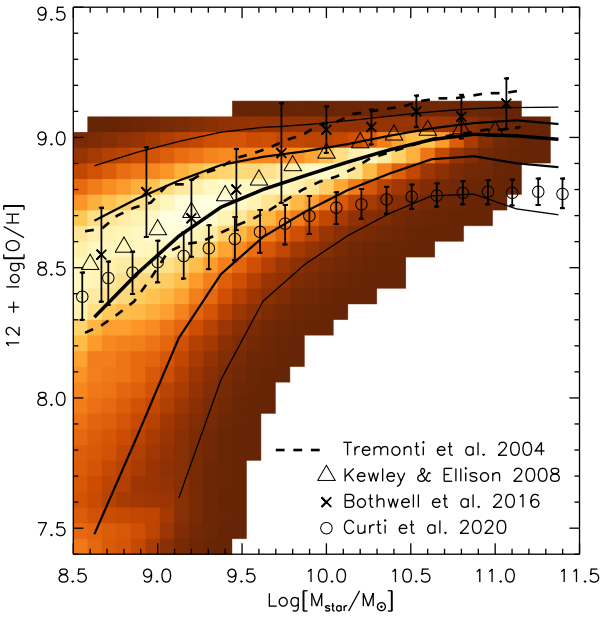

Figure 1. Cold gas metallicity as a function of galaxy stellar mass, as predicted by our model (coloured distribution) and compared with different observational measurements (symbols and dashed lines, as indicated in the legend). The solid black lines correspond to the median and scatter (1σ, and 2σ – ordered by decreasing thickness) of the predicted distribution.

The solid black lines in Fig. 1 show the median, 1σ, and 2σ scatter of the distribution predicted for model star forming galaxies. This particular selection has been used to reflect the fact that our main comparison samples are composed primarily of star-forming galaxies. Specifically, we have selected model star forming galaxies imposing a cold gas fraction of at least 25 per cent, and a specific star formation rate larger than $0.3/t_H$ (with t_H equal to the Hubble time). These galaxies will represent the model sample used throughout this paper (unless otherwise specified). We have verified that results do not change significantly by increasing the threshold adopted for the gas fraction, but this tends to remove the most massive galaxies, and preferentially those with largest metallicity (as we will show below). As in Xie et al. (2017), we remove Helium (26 per cent of the total gas mass) to get the abundance of atomic hydrogen for our model galaxies. The figure shows that model predictions are in quite good agreement with observational measurements based on strong emission lines or photoionization models, both in terms of normalization and overall shape of the mass–metallicity relation. The predicted scatter is larger than observed, particularly for galaxies with stellar mass smaller than $\sim 10^{10}\,M_\odot$ and with metallicity below the median, i.e. the distribution of model metallicities is somewhat more skewed than observed.

Fig. 2 shows the distribution of the same star forming model galaxies in the galaxy stellar mass–gas metallicity plane but colour-coded as a function of the median value of the SFR (top left-hand panel), cold gas mass (top right-hand panel), molecular gas mass (bottom left-hand panel), and atomic gas mass (bottom right-hand panel). The figure clearly shows that all quantities considered contribute to some extent to the scatter of the mass–metallicity relation. Lines of constant star formation rate (and molecular gas content) are almost vertical, i.e. at fixed galaxy stellar mass, there

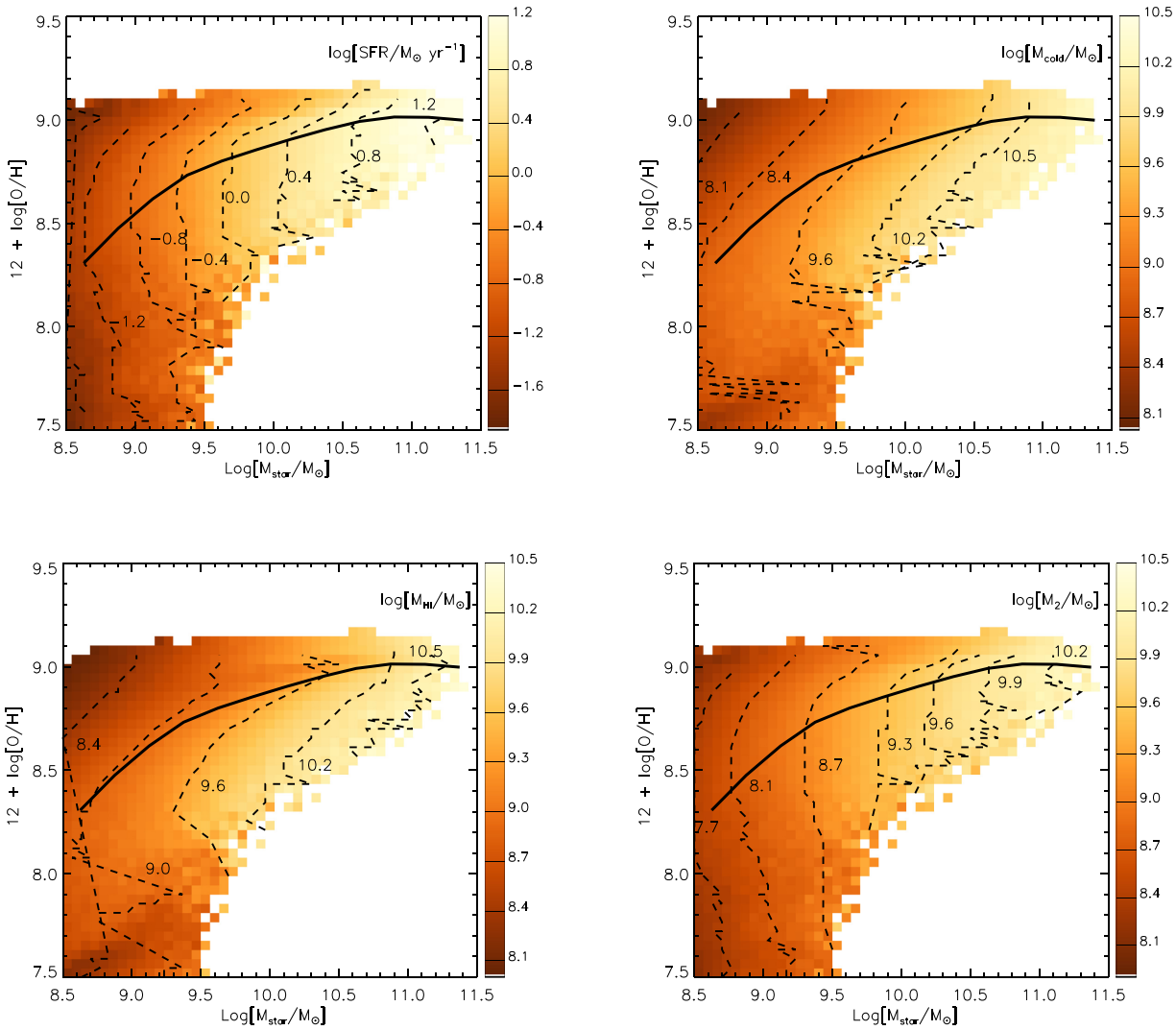

Figure 2. As in Fig. 1, but colour-coded as a function of the median of the quantity indicated on the top right-hand side of each panel. The black solid line shows the median mass–metallicity relation obtained for all star-forming model galaxies considered (see the text for details). Dashed lines show the location of star-forming galaxies whose median value of the quantity indicated on the top right-hand panel is close (within 0.3 dex) to that indicated close to each line.

is only a weak dependence of the cold gas metallicity on the star formation rate or on the molecular gas content. The dependence is stronger for the total amount of gas or the mass of atomic gas that represents its largest fraction. It is not surprising that the trends predicted for the star formation rate are very similar to those obtained for the molecular gas as, in our model, these two quantities are directly related (Xie et al. 2017). In the following, we compare in more detail our model predictions with results from recent observational work.

Fig. 3 shows the offset from the best-fitting mass–metallicity relation as a function of the molecular hydrogen mass. Observational measurements by Bothwell et al. (2016) are shown as symbols and are colour-coded as a function of galaxy stellar mass, as indicated in the legend. Open symbols highlight data with only upper limits for the molecular mass estimates. The latter are based on a CO to H_2 conversion factor that depends on metallicity. Solid lines of different colours show model predictions for the same galaxy stellar mass bins considered for the data. For both the model and observational samples, metallicity offsets have been computed evaluating, for each galaxy, the median metallicity of all galaxies in the sample with very similar galaxy mass (within ±0.05 dex) and the corresponding difference from the predicted and observed best-fitting mass–metallicity relation, respectively. As in Fig. 1, and for consistency with our model sample, we have considered only galaxies in the local Universe from the sample presented in Bothwell et al. (2016). This leaves only about 160 galaxies, which is significantly smaller than the number of model galaxies considered. Albeit statistically small, the observed sample exhibits a weak trend of increasing (negative) offsets with increasing gas mass, within each galaxy mass bin. The trend is qualitatively similar to that obtained for model galaxies. The dispersion of the metallicity offsets decreases with increasing molecular mass, both for the observed and model galaxies. In addition, consistently with findings by Bothwell et al. (2016), we find a mild decrease of the average metallicity offset with increasing molecular mass.

Figs 4 and 5 show a comparison with the recent work by Curti et al. (2020). In Fig. 4, both the observed (dotted lines) and model galaxy samples (solid lines) are binned as a function of the total galaxy

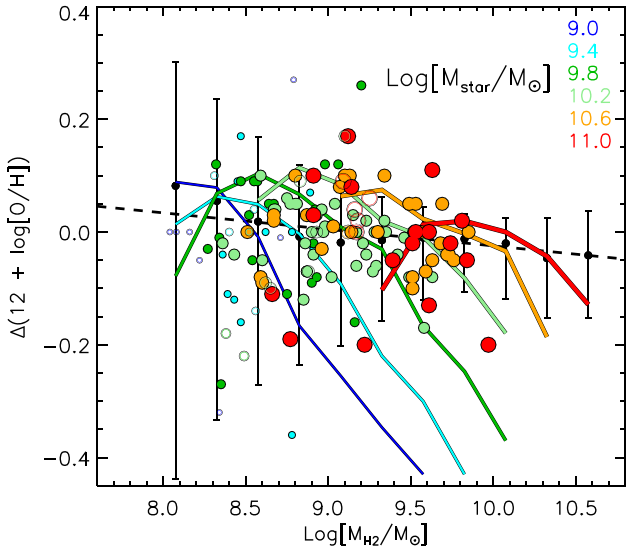

Figure 3. Offset from the mass–metallicity relation as a function of the molecular hydrogen mass. Symbols show observational measurements by Bothwell et al. (2016), and are colour-coded as a function of the galaxy stellar mass as indicated in the legend (the size of the symbols increases with galaxy stellar mass). Open symbols highlight data for which only upper limits for the molecular mass estimates are available. Solid lines, of thickness increasing with increasing galaxy stellar mass, show model predictions for the same galaxy mass bins considered for the data. Black symbols with error bars show the median and percentiles (16th and 84th) obtained for the model sample, independently of the galaxy stellar mass. The dashed line represents a linear fit to the black circles.

star formation rate, as indicated by the legend. A constant vertical shift of −0.22 has been applied to model predictions (the value has been chosen to reproduce approximately the normalization of the relation observed for the most massive galaxies). In the data, the star formation rate is determined from the extinction-corrected Hα luminosity inside the SDSS fibre, and using aperture corrections by Salim et al. (2007). Observational estimates for both stellar masses and star formation rates have been re-scaled to a Chabrier IMF, which is the same adopted in our model. The figure shows that model predictions follow qualitatively the observed trends, but the significance of the SFR dependence is somewhat weaker in the model, that also predicts a steeper slope of the mass–metallicity relation. The overall normalization is different: As discussed above, predictions from our model are in better agreement with measurements based on strong emission lines and photoionization methods. We have verified that, accounting for typical observational uncertainties in the measurements[1] of galaxy stellar masses and galaxy star formation rates removes the dependence predicted for the five to six bins with lowest star formation rates (which is similar to the trends observed in the data).

Fig. 5 shows the relation between gaseous metallicity and star formation rate, for different stellar mass bins. As in the previous figure, observational measurements are shown as dotted lines and model predictions as solid lines. Also in this case, we have applied a constant vertical shift of −0.22. This works relatively well for the most massive bins considered, but brings model predictions significantly below the observational estimates for the least massive galaxies considered. Model predictions exhibit an inversion at star formation rates below Log(SFR/M$_\odot$ yr^{-1}) ∼ −1. Very few such low estimates are available in the observational sample, and we have verified that the trends would flatten when accounting for observational uncertainties on the estimate of the star formation rate.

Fig. 6 shows a comparison between our model predictions and observational estimates by Brown et al. (2018) in terms of the differences of a given parameter (in this specific case, the atomic hydrogen mass $M_{\rm H\,I}$ and the star formation rate) from the value of the same quantity on the mass–metallicity relation, at fixed galaxy stellar mass. Different stellar mass bins are shown in the top and bottom panels, with observational estimates marked by empty symbols connected by dashed lines and model predictions shown as filled symbols connected by solid lines. The latter have been estimated with respect to the best-fitting mass–metallicity relation measured for model galaxies. We only show observational estimates corresponding to the total star formation estimates by Salim et al. (2016) and to the metallicity calibration by Tremonti et al. (2004), which provides a good agreement with our predicted mass–metallicity relation. In the left-hand panels, the dashed lines correspond to the inverse one-to-one relation, to guide the eye. Our model predicts trends that are qualitatively similar to those observed, with a few important differences, that can be summarized as follows:

(i) The metallicity offsets predicted by our model extend to more negative values than the observational data, i.e. there are more significant deviations below the mass–metallicity relation in the model. This is consistent with the large scatter towards low metallicities shown for our model galaxies in Fig. 1.

(ii) For galaxies that are offset above the mass–metallicity relation (positive values of $\Delta\, Z_{\rm gas}$), our model predicts a stronger dependence on the star formation rate than observed, with smaller (more negative) offsets from the average values of the star formation rate on the mass–metallicity relation.

4 WHICH PHYSICAL PROCESSES DRIVE THE OBSERVED SECONDARY DEPENDENCES?

The results discussed above show that our model provides a good agreement with observational measurements of the mass–metallicity relation in the local Universe, as well as of the related secondary dependence trends. The agreement is not perfect, but the main trends are qualitatively reproduced. This confirms that our model represents an ideal tool to investigate their origin in a cosmological context, and to quantify the relative importance of different physical processes.

In order to characterize the evolution of our model galaxies and identify the physical processes that are driving the trends discussed above, we have analysed in detail the evolution of individual model galaxies by following their main progenitor branch, and saving all relevant information about the flows of gas and metals driven by different physical processes. For the analysis presented in this section, we have focused only on central galaxies. These represent, overall, the largest fraction (∼67 per cent) of the model star-forming galaxies considered in Section 3. Fig. 7 shows the trajectories of a few example galaxies in the galaxy stellar mass–gas metallicity plane in the top panels, and the corresponding evolution of the cold gas mass (green thick lines) and gaseous metallicity (black lines) in the bottom panels. We have selected galaxies in a narrow bin of galaxy stellar mass ($\log M_{\rm star}/{\rm M}_\odot = 10.0$–$10.4$), and considered example galaxies whose trajectories in the mass–metallicity plane are either relatively close (dashed lines) or distant (dotted lines) from the present-day best-fitting $\log M_{\rm star}/{\rm M}_\odot = 10.0$–$10.4$ relation, for

[1]In this case, we have simply convolved model predictions assuming a Gaussian uncertainty on $\log M_\star$ and log SFR of 0.15–0.20.

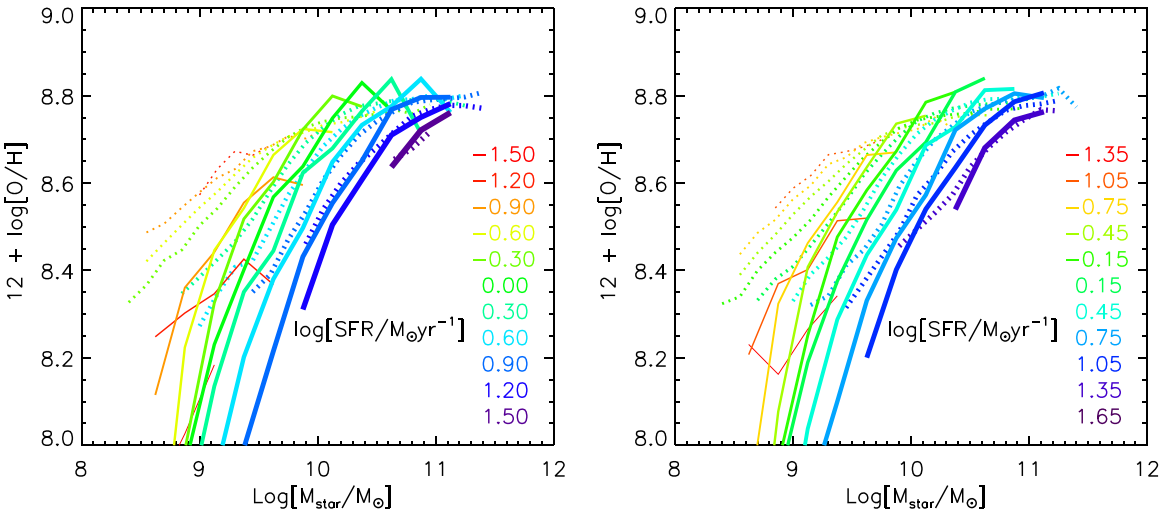

Figure 4. Cold gas metallicity as a function of galaxy stellar mass, for bins of galaxies with different star formation rates as indicated in the legend. Dotted lines show observational measurements by Curti et al. (2020), while solid lines show predictions based on our reference model. The line thickness increases with increasing values of the star formation rate. A constant vertical shift of −0.22 has been applied to all model predictions. These have *not* been convolved with observational uncertainties. When this is done, the dependence on star formation rates disappears for the five to six bins with lowest star formation rates, while the trends shown for bins with larger star formation rates are not significantly affected.

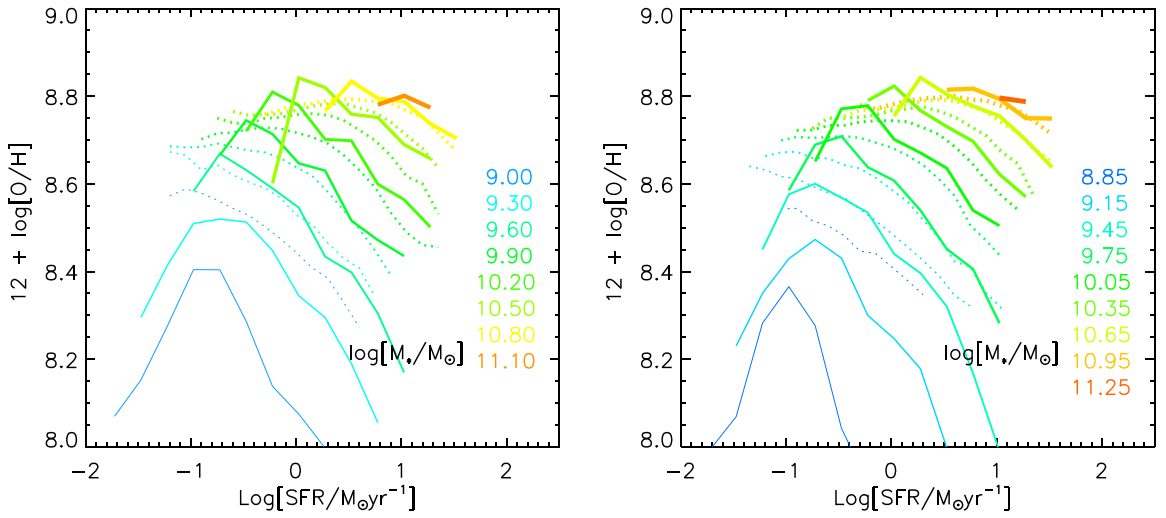

Figure 5. Cold gas metallicity as a function of galaxy star formation rate, for bins of galaxy stellar mass as indicated in the legend. Dotted lines show observational measurements by Curti et al. (2020), while model predictions are shown as solid lines. The line thickness increases with increasing galaxy stellar mass. As in Fig. 4, a constant vertical shift of −0.22 has been applied to model predictions. These have *not* been convolved with observational uncertainties. We have verified that accounting for such uncertainties would flatten the trends at low star formation rates.

a significant fraction of the galaxies lifetimes. The solid lines show instead intermediate cases, and represent the most frequent behaviour we find for the model galaxies whose trajectories we have inspected by eye, independently of galaxy stellar mass and offset from the best-fitting relation. Our model galaxies show a large variety of possible paths in the mass–metallicity plane, which are determined by a complex interplay between different physical processes. While the galaxy stellar mass increases monotonically with time, the gaseous metallicity experiences significant oscillations. Only for a minority of the galaxies inspected, we find evolutionary tracks that oscillate around the mass–metallicity relation that is predicted at $z = 0$. Most of the tracks lie even below the mass–metallicity relation predicted at higher redshift (in fact, the evolution is rather weak, as will be discussed in detail in a forthcoming paper). The variety of tracks predicted by our model reflects the complex interplay between the different physical processes driving the chemical enrichment of the interstellar medium.

The bottom panels of Fig. 7 show that metallicity variations are strongly correlated with variations of the cold gas mass. Specifically, negative variations of gas mass typically correspond to positive variations of metallicity, i.e. the gaseous metallicity increases when the gas decreases. On the other hand, positive variations of gas mass can lead to both an increase or a decrease of the gaseous metallicity.

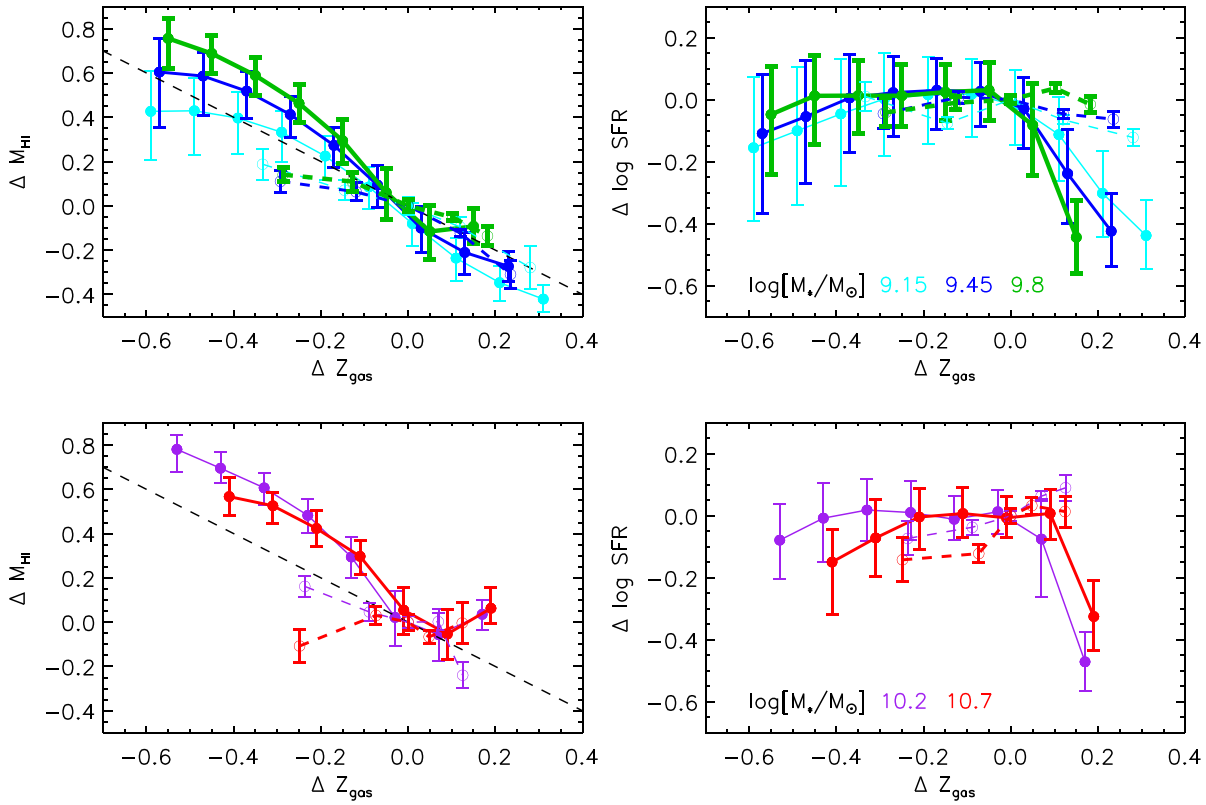

Figure 6. Differences of H I mass (left-hand panels) and star formation rate (right-hand panels) as a function of the differences in metallicity from the value of the same quantities on the mass–metallicity relation. Top and bottom panels show different stellar mass bins, with model predictions shown as filled symbols connected by solid lines and observational estimates by Brown et al. (2018) marked by open circles connected by dashed lines. In all panels, the line thickness increases with increasing galaxy stellar mass.

To evaluate statistical correlations between variations of different physical quantities in our model, we consider all galaxies in the same narrow bin of galaxy stellar mass ($\log M_{\rm star}/{\rm M}_{\odot} = 10.0$–$10.4$), and store all information about variations of cold gas mass, star formation rate, and gaseous metallicity measured by following the main branch (i.e. the branch traced by the most massive progenitor at each redshift). Fig. 8 shows the percentage variations of cold gas mass (top panels) and star formation rates (bottom panels) as a function of the gaseous percentage metallicity variations, measured between two subsequent snapshots of the model outputs. Grey symbols represent a random subset of 10 000 individual variations, covering the redshift range from zero to that of the first main progenitors of the model galaxy sample considered. Contours enclose the regions containing 90 per cent of the percentage variations corresponding to $z < 5.0$, 3.0, 1.5, and 0.5 (in order of increasing line thickness, and colour-coded as indicated in the legend). We have splitted the sample according to their offset from the best-fitting mass–metallicity relation (left- and right-hand panels are used for galaxies in the lower and upper 15th percentile of the distribution, respectively). The figure shows a very weak correlation between variations of the cold gas metallicity and of the star formation rate (bottom panels), while there is a clear correlation between variations of the gas metallicity and of the cold gas mass (top panels). The correlation becomes tighter with decreasing redshift and for negative variations of the metallicity, and is such that decreases/increases of cold gas lead on average to increases/decreases of the cold gas metallicity. The bottom panels of Fig. 8 show that increase in the star formation rate can lead both to positive and negative variations of the cold gas metallicity. The latter case is expected, e.g. during galaxy mergers with gas-rich but low-mass satellites, that in our model would trigger a starburst after the cold gas has been depleted due to the merger. Finally, Fig. 8 also shows that the differences between galaxies that are offset above or below the mass–metallicity relation become clearer, in terms of the differences considered, with decreasing redshift: Galaxies above the mass–metallicity relation tend to have smaller percentage variations of gas mass and star formation rates than their counterparts below the relation. The narrow tilted features that are visible in the lower right-hand side regions of the bottom panels, when looking at the highest redshift contour shown, correspond to variations of the star formation rate following merger-driven bursts. In GAEA, these are modelled using the 'collisional starburst' prescription as introduced by Somerville, Primack & Faber (2001), where the mass of new stars formed is a fixed fraction, that depends on the mass ratio of the merging galaxies, of the gas mass available.

We have verified that the trends shown in Fig. 8 do not depend significantly on galaxy stellar mass, but there is an increase of the relative variations of cold gas mass and metallicity for decreasing galaxy mass.

Using the detailed information saved from our model, we can now address the following question: Which physical processes are determining positive and negative variations of gas, and therefore offset model galaxies below or above the mass–metallicity relation? To address this question, we have considered again galaxies in a narrow mass bin, and only examined those that are at the extreme

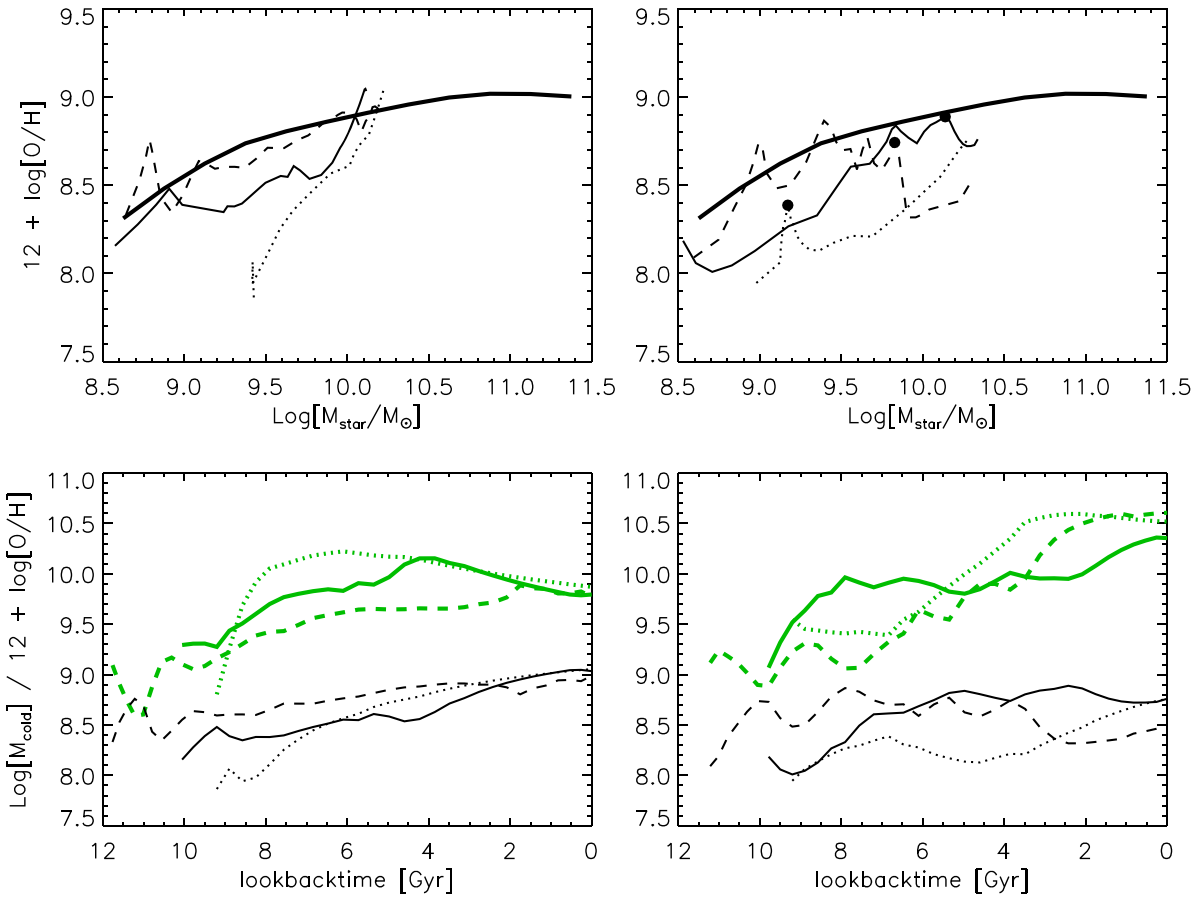

Figure 7. Top panels show the trajectories of a few example galaxies in the stellar mass–gaseous metallicity plane. The left- and right-hand panels are for galaxies offset above and below the mass–metallicity relation, respectively. Dashed and dotted lines correspond to example galaxies whose trajectories are relatively close or distant from the predicted relation at $z = 0$ (thick solid line) for a significant fraction of the galaxy's lifetime. Solid lines correspond to intermediate cases (the most frequent among the model galaxies analysed – see the text). The bottom panels show the corresponding evolution of the cold gas mass (thick green lines) and gaseous metallicity (black lines). The filled circles in the top right-hand panel mark the first metallicity maximum, going backwards in time, identified for each model galaxy (this will be used later in our analysis).

of the distribution (above the 95th percentile, or below the 5th percentile). This selection is aimed at having clearer differences between the two populations, but we have verified that our results do not change qualitatively when using a different selection. Below, we comment explicitly on how the trends found change as a function of galaxy stellar mass.

Let us start from galaxies that deviate above the mass metallicity relation. For each model galaxy, we have followed back its main progenitor and recorded the first time when the main progenitor crosses the best-fit relation of model galaxies at $z = 0$ (see the top left-hand panel of Fig. 7). We have also recorded the variations of gas, between this time and $z = 0$, due to star formation, stellar feedback, gas recycling, gas cooling, and galaxy mergers (in our model, feedback from active galactic nuclei does not affect the amount of cold gas in model galaxies, i.e. does not trigger galactic winds). Among the processes considered, star formation and stellar feedback cause negative variations of cold gas, while all other processes cause positive variations of cold gas mass. In the top panels of Fig. 9, we show the distribution of the lookback times when galaxies with stellar mass between $\log(M_{\rm star}/{\rm M}_\odot) = 10$ and 10.5 (and above the 95th percentiles of the metallicity distribution) cross the best-fitting relation found for model galaxies at $z = 0$. The distribution has a clear and well-defined peak around ∼2 Gyr ago (i.e. $z \sim 0.17$ in our cosmology), with a tail at earlier epochs.

We find that almost all galaxies selected using the above criteria (∼97 per cent of them) experience a negative variation of gas between the time they cross the mass–metallicity relation and the present time. These vary between $\sim 7.5 \times 10^6$ and $\sim 8.5 \times 10^9$ M$_\odot$, with a median of $\sim 2.5 \times 10^9$ M$_\odot$. The bottom panel of Fig. 9 shows the fractional contributions to the absolute variation of gas by different physical processes: the largest contribution, with an average of ∼44 per cent, comes from star formation. For a very small fraction of the galaxies considered (including the ∼3 per cent that experience positive variations of cold gas mass since crossing time), gas cooling contributes slightly more than star formation (∼38 against 34 per cent). Stellar feedback and gas recycling contribute to ∼18–19 per cent of the absolute variation of cold gas mass (the former reduces the cold gas in model galaxies, while the latter increases it). Finally, galaxy mergers represent a negligible contribution for virtually all galaxies considered.

We have also tested if and how much results change as a function of galaxy stellar mass considering a lower ($\log(M_{\rm star}/{\rm M}_\odot) = 9.5$–10.0) and higher ($\log(M_{\rm star}/{\rm M}_\odot) = 10.5$–11.0) stellar mass bin. We find some weak trends as a function of galaxy mass: for lower/higher mass

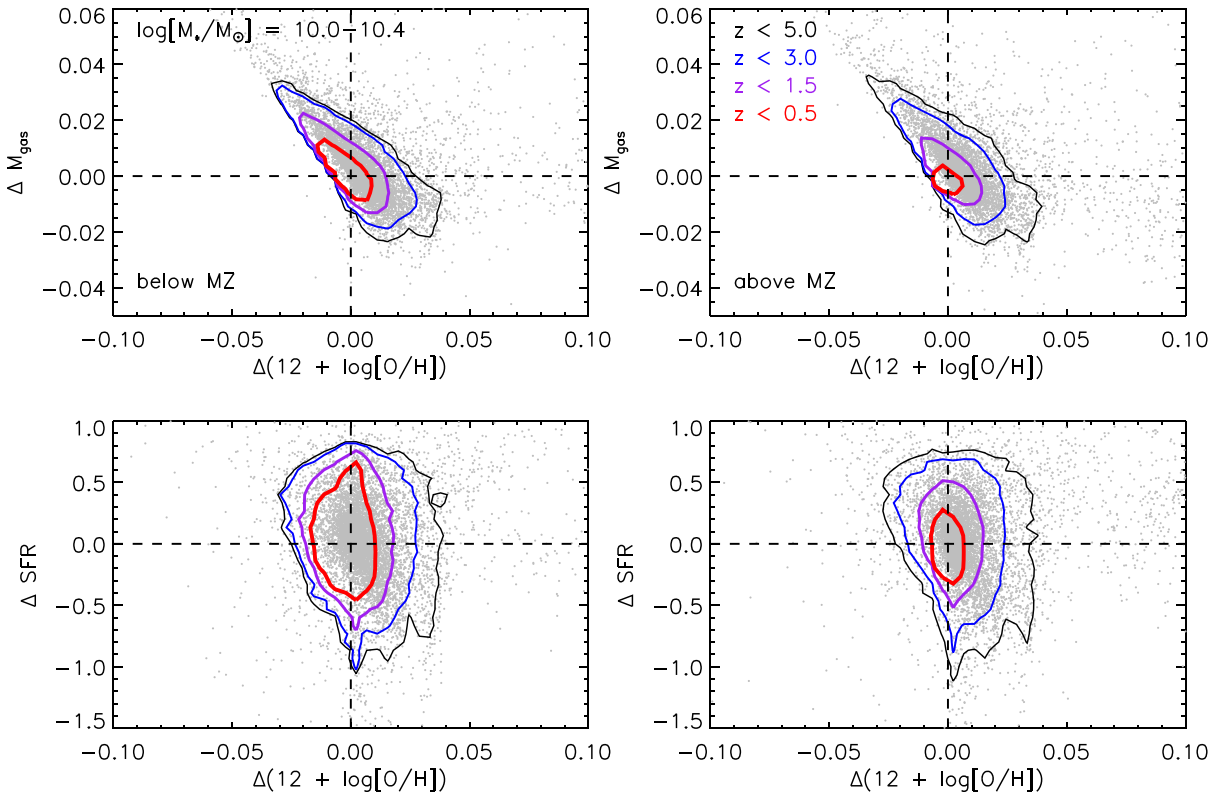

Figure 8. Percentage variations of cold gas mass (top panels) and star formation rate (bottom panels) as a function of variations of cold gas metallicity, for galaxies with stellar mass between $10^{10.2}$ and $10^{10.4}\,M_{\odot}$. The left- and right-hand panels are for galaxies offset below and above the model best-fitting mass–metallicity relation (the lower/upper 15th percentile), respectively. Grey symbols represent a random subset of 10 000 individual variations, covering the redshift range from zero to the highest redshift at which progenitors of model galaxies are found. Contours show regions including 90 per cent of the points at $z < 5.0,\ 3.0,\ 1.5,$ and 0.5, in order of increasing thickness and colour-coded as indicated in the legend. Dashed lines are plotted to guide the eye.

galaxies, the tail towards early crossing times of the mass–metallicity relation tends to be more/less pronounced, respectively. The fractional contribution from star formation is largest (∼53 per cent) for the most massive sample, where we find that 100 per cent of the galaxies considered experience a negative variation of gas between the time when their progenitors cross the mass–metallicity relation and today. The equivalent of Fig. 9 for the other two galaxy mass bins considered are provided in Appendix A.

As discussed earlier, negative variations of gas are always associated with positive variations of metallicity. In our model, stellar feedback removes a fraction of the cold gas reheating or ejecting it. We assume that this occurs leaving the metallicity of the cold gas component unchanged which means that, in our model, positive variations of metallicity can only be caused by star formation. Therefore, *late star formation, and the corresponding metal production, is primarily responsible for the offset of galaxies above the mass metallicity relation*.

Let us now move to galaxies that are offset below the mass–metallicity relation. We again consider galaxies with stellar mass between $\log(M_{\rm star}/M_{\odot}) = 10$ and 10.5, but now select only those that are below the 5th percentile of the metallicity distribution. In this case, we trace the main progenitor of each model galaxy backward in time, up to the time corresponding to the most recent maximum of the cold gas metallicity. For the example galaxies shown in Fig. 7, these times are marked as filled circles. We then compute the variations of gas due to different physical processes between the time just defined and present. Results are shown in Fig. 10. The distribution of the times corresponding to the last maximum value of the cold gas metallicity peaks at ∼2.5 Gyr, but has a broad tail that extends up to 10 Gyr ago.

All galaxies considered in this case experience a positive variation of the cold gas, with the largest contribution (∼60 per cent on average) coming from gas cooling. The contributions from star formation, stellar feedback, and gas recycling are significantly lower (and also lower than the corresponding contributions found for galaxies that are offset above the mass–metallicity relation). Also in this case, galaxy mergers represent a negligible contribution to the absolute variation of cold gas.

We have verified if there is a dependence on galaxy stellar mass: for less and more massive galaxies, the tail of the distribution of the times of maximum metallicity becomes more and less pronounced at early cosmic epochs, respectively. In addition, the contributions from star formation and recycling tend to decrease/increase for less/more massive galaxies, against a larger/smaller fractional contribution from gas cooling. For the least massive bin considered, a very small fraction of the galaxies (∼3 per cent) experience a negative variation (i.e. a reduction) of the cold gas available. For these galaxies, the fractional contribution of star formation is actually larger than that of gas cooling (i.e. they behave like the galaxies analysed in Fig. 9).

As discussed earlier, positive variations of cold gas can be associated with both positive and negative variations of metallicity.

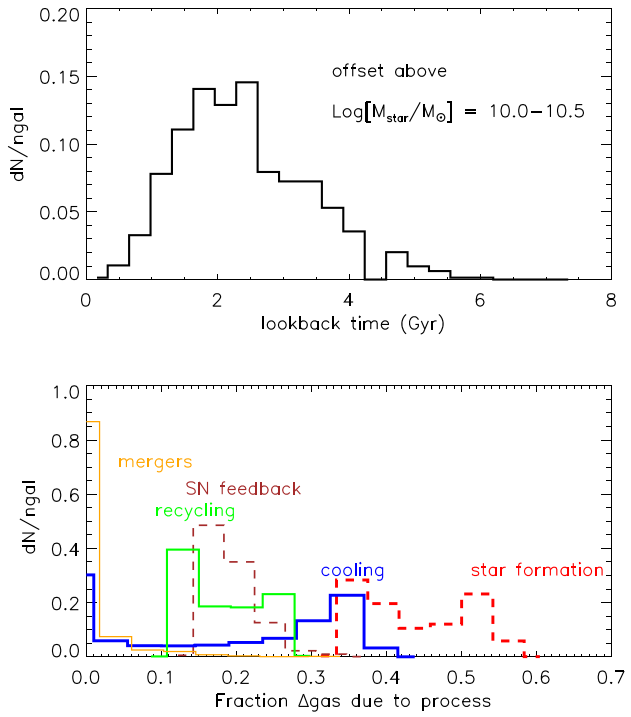

Figure 9. The top panel shows the distribution of the lookback times when the main progenitor crosses (for the first time going backward in time) the best-fitting relation found for model galaxies at $z = 0$. The bottom panel shows the fractional contributions of different physical processes to the absolute variation of cold gas in model galaxies, between the crossing time defined above and today. Contributions from processes that cause negative/positive variations of the cold gas mass are shown with dashed/solid lines. Increasing line thickness is used for stellar feedback, star formation (that cause negative variations of cold gas) and mergers, recycling and cooling (that lead to positive variations of cold gas).

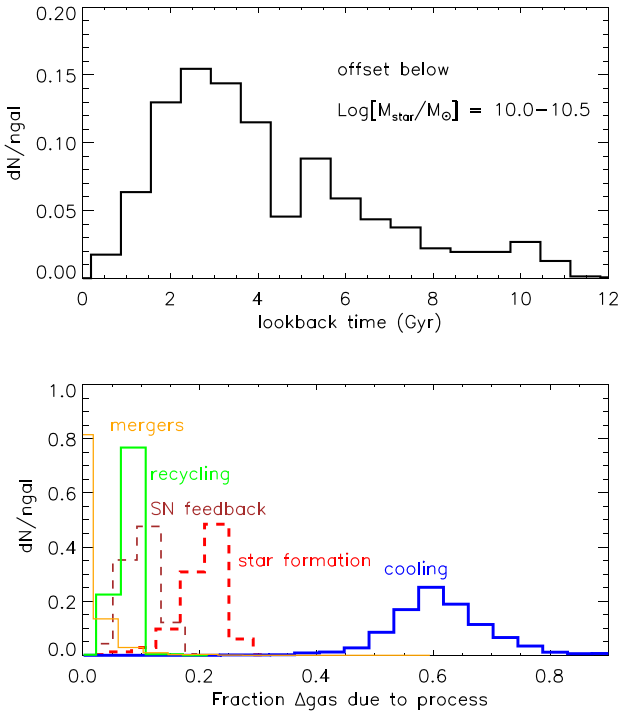

Figure 10. The top panel shows the distribution of the lookback times corresponding to the most recent maximum value of the cold gas metallicity. The bottom panel shows, as in Fig. 9, the fractional contributions of different physical processes to the absolute variation of cold gas, between the time defined above and today. As for Fig. 9, we have highlighted with dashed histograms the contributions of physical processes causing negative variations of the cold gas.

Our analysis indicates that, in most cases, *offsets below the mass metallicity relation can be explained by dilution of cold gas due to late gas cooling*.

It should be noted that the galaxy samples used for Figs 9 and 10 do not have the same distribution of galaxy stellar mass. In particular, galaxies offset above the mass–metallicity relation tend to be on average more massive than galaxies offset below the relation. We have verified that the trends discussed above remain qualitatively the same when using mass matched samples. In this case, we find that galaxies that are offset below the mass–metallicity relation at $z = 0$ tend to reside in slightly more massive haloes ($\log M_{\rm halo}/{\rm M}_\odot \sim 11.85$) than galaxies of the same mass that are found above the mass–metallicity relation (for these galaxies, $\log M_{\rm halo}/{\rm M}_\odot \sim 11.6$). This halo mass difference appears at low redshift ($\lesssim$0.4) and leads to an increase of the gas cooling (and therefore of the cold gas masses) in galaxies below the mass–metallicity relation. This late gas cooling also leads to larger radii, lower molecular to atomic mass ratios, and lower star formation rates. We find that these trends are independent of the stellar mass bin considered, but more prominent for low- and intermediate-mass galaxies. This suggests that AGN feedback, whose efficiency instead increases with increasing galaxy mass, plays a negligible role in suppressing cooling for galaxies that are found above the mass–metallicity relation. Therefore, the scatter above the relation is due to a lack of late gas accretion, rather than to an excess of star formation.

One final question that we can address using results from our model is to what extent late gas cooling is due to cosmological infall or re-incorporation of gas that has been previously ejected due to stellar feedback. We show the relevant information in Fig. 11. The three panels correspond to three different stellar mass bins considered. In each panel, we show the distributions of the variations of the hot gas (solid black histograms), the ejected gas (dotted cyan), the cooling gas (dot–dashed blue), the infalling gas (dashed red), and the re-incorporated gas (long dashed brown). As for Fig. 10, variations are defined between the time corresponding to the last maximum metallicity value and the present time. The figure shows that for the lowest and intermediate stellar mass bins considered, the largest contribution is coming from re-incorporation of gas that has been previously ejected outside the galaxy haloes. For the most massive bins, the absolute value of the contribution from cosmological infall increases, and the relative importance of this channel becomes comparable to that of gas re-incorporation. The behaviour seen in Fig. 11 is a consequence of our assumption that re-incorporation time-scales are inversely proportional to halo mass (Hirschmann et al. 2016, and references therein). As discussed in that work (see their Fig. 4), in our model, gas re-accretion is suppressed at early cosmic epochs and is delayed to progressively lower redshifts for galaxies of decreasing stellar mass. Since the ejection occurs at much earlier times than re-incorporation, the material that is re-accreted is relatively metal-poor, leading to a dilution of the cold gas metallicity. In particular, we find that the average metallicity of the re-incorporated gas is about 0.4–0.5 times that of the hot gas for re-incorporation events that occur below $z \sim 1$.

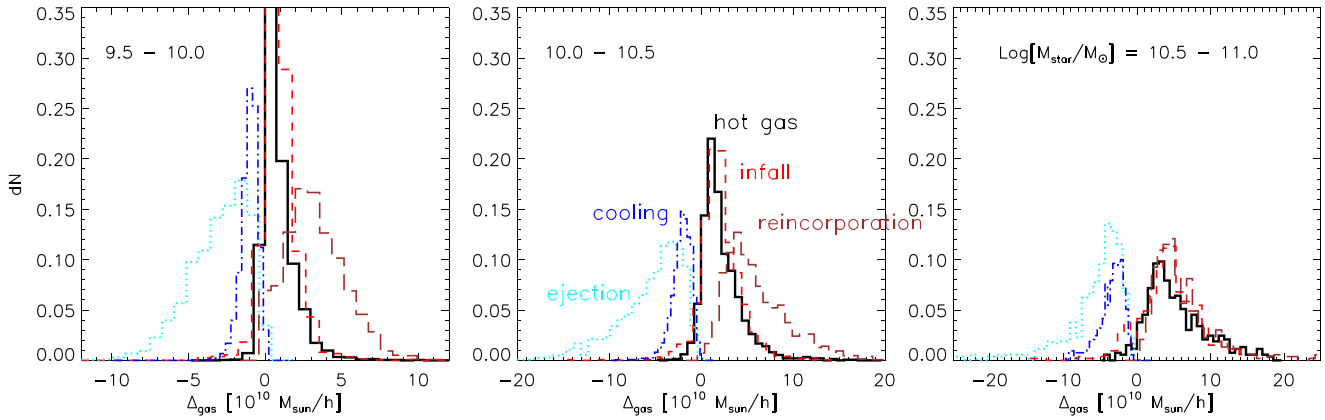

Figure 11. Variations of hot gas (black solid histograms), cosmologically infalling gas (dashed red), ejected gas (dotted cyan), cooling gas (dot–dashed blue), and re-incorporated gas (long-dashed brown), between the time corresponding to the last maximum metallicity value and the present time. The three panels correspond to different galaxy stellar mass bins, as indicated in the legend.

5 DISCUSSION AND CONCLUSIONS

In this paper, we have taken advantage of the state-of-the-art GAEA semi-analytic model (Hirschmann et al. 2016) to analyse the origin of secondary dependencies in the observed correlation between galaxy stellar mass and cold gas metallicity. Our model reproduces well the observed evolution of the relation up to $z \sim 2$ (Hirschmann et al. 2016; Xie et al. 2017), and includes an explicit treatment for the partition of the cold gas in its atomic and molecular components (Xie et al. 2017). This has allowed us to carry out a detailed comparison with the trends observed in the local Universe, where the existence of a secondary dependence in the mass–metallicity relation has been studied as a function of different physical properties, including galaxy star formation rate and gas content (both atomic and molecular).

Our model reproduces relatively well, both in terms of normalization and shape, measurements of the mass–metallicity relation in the local Universe based on strong emission lines. The model also reproduces qualitatively well the trends measured as a function of star formation rate and of different gas-phase components (Bothwell et al. 2016; Brown et al. 2018; Curti et al. 2020). Specifically, the predicted offsets from the mass–metallicity relation depend weakly on the star formation rate and mass of the molecular gas, while the correlation is stronger with the atomic gas mass. Therefore, in agreement with what is inferred in the local Universe, the cold gas content of our model galaxies (whose largest fraction is represented by the atomic phase) can be considered as the third parameter governing the scatter of the mass–metallicity relation.

As argued in previous work (see e.g. discussion in Brown et al. 2018, and references therein), the observed trends can be explained with fluctuations of the gas accretion rates: a decrease of the gas supply leads to an increase of the gas metallicity as star formation progresses, while an increase of the available gas (due to e.g. gas cooling following cosmological infall, or galaxy–galaxy mergers) would generally lead to a dilution of the cold gas metallicity. This picture is supported by several theoretical studies, both based on the explicit *ansatz* of equilibrium between gas inflow, outflows, and star formation (e.g. Davé et al. 2012; Lilly et al. 2013), and not assuming equilibrium (e.g. Dayal et al. 2013; Forbes et al. 2014). These studies, however, cannot explain the origin of the fluctuations of gas supply, or distinguish between cosmological infall and re-accretion of gas that has been previously ejected by galactic outflows.

In our model, galaxies that experience negative variations of gas due to star formation, without the cold gas reservoir being replenished by additional gas cooling, move along diagonal lines in a mass–metallicity plane (towards larger masses and larger metallicities). As we have shown in the previous section, this implies that galaxies that are offset above the mass–metallicity relation have been driven there primarily by star formation. The contribution from stellar feedback that, in our model, only reduces the mass of cold gas but does not alter its metallicity is however not negligible. In a scenario where metals are selectively lost via galactic winds, stellar feedback would reduce the cold gas amount and also its metallicity. Thus, the contribution from star formation and stellar feedback in determining variations of the cold gas metallicity would be more similar, in absolute terms. The fractional contribution of star formation to late changes of cold gas mass is stronger for more massive star-forming galaxies, since they are characterized by higher star formation rates and deeper potential wells that make gas removal by star formation less efficient. The characteristic time-scales of the metallicity variation are, in this case, relatively long because the star formation efficiency is generally only of the order of few per cent. Therefore, galaxies that are found above the mass–metallicity relation have 'crossed' it relatively recently (for our model galaxies, this happened on average ∼2 Gyr ago).

Positive variations of gas can lead to both positive and negative variations of the cold gas metallicity. The former take place during early phases of galaxy evolution and are driven by gas recycling and, to a minor extent, by mergers with other gas-rich galaxies. The latter can occur in case of metallicity dilution driven by either new supply of cold material (gas cooling) or by mergers with lower mass, and therefore lower metallicity, galaxies. All our model galaxies that are offset below the mass–metallicity relation in the local Universe have experienced positive variations of cold gas, which are due to gas cooling. More specifically, we find that the largest contribution to the newly cooling gas is from material that has been previously ejected via stellar feedback, for galaxies with stellar mass lower than $\sim 10^{10.5}\,M_{\odot}$. For more massive galaxies, the relative contribution from this 'ejected' component decreases and becomes comparable to that due to cosmological infall of gas. This trend is, in our model, a consequence of specific assumptions about the re-incorporation time-scales (Hirschmann et al. 2016, and references therein). Negative variations of the cold gas metallicity occur on time-scales that are

shorter than those associated with positive variations of metallicity, and are essentially determined by the cooling time-scales.

The stochasticity of halo merger histories leads to a wide range of possible trajectories in the mass–metallicity plane. Albeit some general trends can be found and an 'average' behaviour can be described analytically, a full understanding of the scatter in the observed mass–metallicity relation requires cosmologically embedded galaxy formation models, like the one considered here. In this work, we have focused on the local Universe and on the origin of secondary dependences in the mass–metallicity relation. In future work, we plan to investigate if and how model predictions vary as a function of cosmic time and how this evolution depends on the specific assumptions made for stellar feedback.

ACKNOWLEDGEMENTS

We thank Filippo Mannucci, Mirko Curti, and Toby Brown for providing us their observational measurements in electronic format. FF acknowledges support from the PRIN MIUR project 'Black Hole winds and the Baryon Life Cycle of Galaxies: the stone-guest at the galaxy evolution supper', contract 2017-PH3WAT. MH acknowledges financial support from the Carlsberg Foundation via a 'Semper Ardens' grant (CF15-0384). We also thank Filippo Mannucci and Mirko Curti for useful and constructive comments on a preliminary version of this paper.

DATA AVAILABILITY

The model data underlying this paper will be shared on request to the corresponding author.

An introduction to GAEA, a list of our recent work, as well as data files containing published model predictions, can be found at http://adlibitum.oats.inaf.it/delucia/GAEA/.

REFERENCES

Blitz L., Rosolowsky E., 2006, ApJ, 650, 933
Boselli A., Cortese L., Boquien M., 2014, A&A, 564, A65
Bothwell M. S. et al., 2014, MNRAS, 445, 2599
Bothwell M. S., Maiolino R., Peng Y., Cicone C., Griffith H., Wagg J., 2016, MNRAS, 455, 1156
Brown T., Cortese L., Catinella B., Kilborn V., 2018, MNRAS, 473, 1868
Chabrier G., 2003, PASP, 115, 763
Chisholm J., Tremonti C., Leitherer C., 2018, MNRAS, 481, 1690
Collacchioni F., Cora S. A., Lagos C. D. P., Vega-Martínez C. A., 2018, MNRAS, 481, 954
Curti M., Cresci G., Mannucci F., Marconi A., Maiolino R., Esposito S., 2017, MNRAS, 465, 1384
Curti M., Mannucci F., Cresci G., Maiolino R., 2020, MNRAS, 491, 944
Dalcanton J. J., 2007, ApJ, 658, 941
Davé R., Finlator K., Oppenheimer B. D., 2012, MNRAS, 421, 98
Dayal P., Ferrara A., Dunlop J. S., 2013, MNRAS, 430, 2891
De Lucia G., Blaizot J., 2007, MNRAS, 375, 2
De Lucia G., Tornatore L., Frenk C. S., Helmi A., Navarro J. F., White S. D. M., 2014, MNRAS, 445, 970
De Rossi M. E., Bower R. G., Font A. S., Schaye J., Theuns T., 2017, MNRAS, 472, 3354
Fontanot F., Hirschmann M., De Lucia G., 2017, ApJ, 842, L14
Forbes J. C., Krumholz M. R., Burkert A., Dekel A., 2014, MNRAS, 443, 168
Guo Q. et al., 2011, MNRAS, 413, 101
Hirschmann M., De Lucia G., Fontanot F., 2016, MNRAS, 461, 1760
Hughes T. M., Cortese L., Boselli A., Gavazzi G., Davies J. I., 2013, A&A, 550, A115
Kewley L. J., Dopita M. A., 2002, ApJS, 142, 35
Kewley L. J., Ellison S. L., 2008, ApJ, 681, 1183
Köppen J., Edmunds M. G., 1999, MNRAS, 306, 317
Köppen J., Weidner C., Kroupa P., 2007, MNRAS, 375, 673
Kroupa P., 2001, MNRAS, 322, 231
Lagos C. d. P. et al., 2016, MNRAS, 459, 2632
Lara-López M. A. et al., 2010, A&A, 521, L53
Larson R. B., 1974, MNRAS, 169, 229
Lequeux J., Peimbert M., Rayo J. F., Serrano A., Torres-Peimbert S., 1979, A&A, 80, 155
Lilly S. J., Carollo C. M., Pipino A., Renzini A., Peng Y., 2013, ApJ, 772, 119
McClure R. D., van den Bergh S., 1968, AJ, 73, 1008
Maiolino R. et al., 2008, A&A, 488, 463
Maiolino R., Mannucci F., 2019, A&AR, 27, 3
Mannucci F., Cresci G., Maiolino R., Marconi A., Gnerucci A., 2010, MNRAS, 408, 2115
Onodera M. et al., 2016, ApJ, 822, 42
Saintonge A. et al., 2011, MNRAS, 415, 32
Salim S. et al., 2007, ApJS, 173, 267
Salim S. et al., 2016, ApJS, 227, 2
Sanders R. L. et al., 2020, MNRAS, 491, 1427
Skillman E. D., Kennicutt R. C., Hodge P. W., 1989, ApJ, 347, 875
Somerville R. S., Davé R., 2015, ARA&A, 53, 51
Somerville R. S., Primack J. R., Faber S. M., 2001, MNRAS, 320, 504
Springel V. et al., 2005, Nature, 435, 629
Torrey P. et al., 2019, MNRAS, 484, 5587
Tremonti C. A. et al., 2004, ApJ, 613, 898
Troncoso P. et al., 2014, A&A, 563, A58
Wang J., De Lucia G., Kitzbichler M. G., White S. D. M., 2008, MNRAS, 384, 1301
Xie L., De Lucia G., Hirschmann M., Fontanot F., Zoldan A., 2017, MNRAS, 469, 968
Yates R. M., Kauffmann G., Guo Q., 2012, MNRAS, 422, 215
Zahid H. J., Kewley L. J., Bresolin F., 2011, ApJ, 730, 137
Zaritsky D., Kennicutt R. C., Jr, Huchra J. P., 1994, ApJ, 420, 87

APPENDIX A: DEPENDENCE ON GALAXY STELLAR MASS

In Section 4, we have discussed how the trends discussed for galaxies that are offset above or below the mass–metallicity relation depend on galaxy stellar mass. For completeness, we provide in this appendix the equivalents of Figs 9 and 10 for galaxies more and less massive than those considered in the main text. Specifically, the top panels of Figs A1 and A2 show the distribution of the lookback times when the main progenitors cross the best-fitting mass–metallicity relation, found for model galaxies at $z = 0$. The bottom panels show the fractional contributions of different physical processes to the absolute variation of cold gas experienced by model galaxies between the crossing time and today. Fig. A1 corresponds to galaxies with stellar mass between $\log(M_{\rm star}/{\rm M}_{\odot}) = 9.5$ and 10, while Fig. A2 is for galaxies with stellar mass between $\log(M_{\rm star}/{\rm M}_{\odot}) = 10.5$ and 11.

Figs A3 and A4 show, for the same galaxy mass bins, the distributions of the lookback times corresponding to the most recent maximum values of the cold gas metallicity (top panels), and the fractional contributions of different physical processes to the absolute variation of cold gas experienced by model galaxies between this time and today (bottom panels).

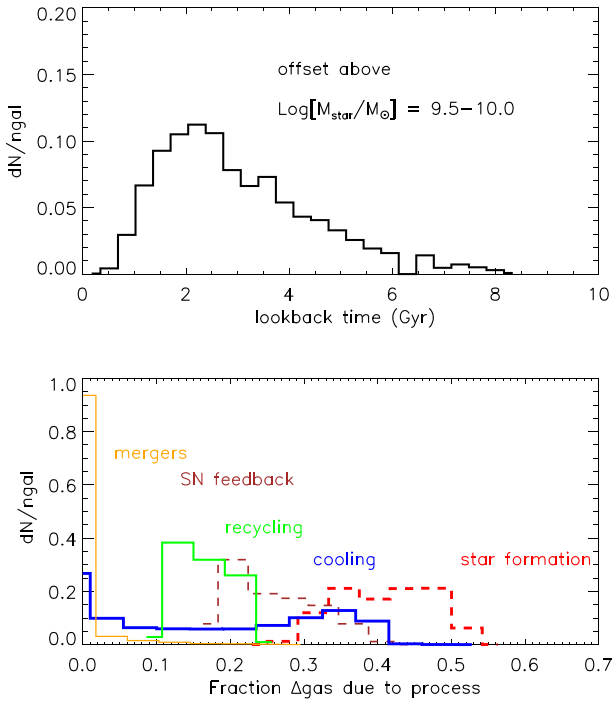

Figure A1. As in Fig. 9, but for galaxies with stellar mass between $\log(M_{\rm star}/{\rm M}_{\odot}) = 9.5$ and 10.

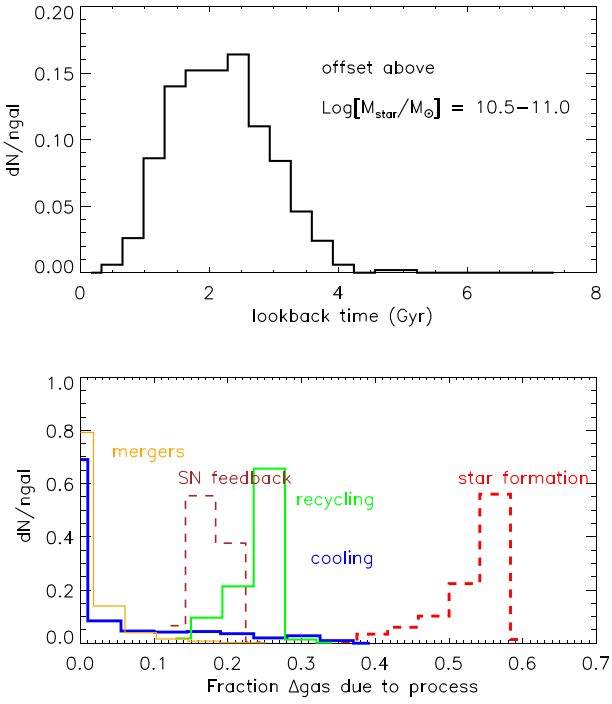

Figure A2. As in Fig. 9, but for galaxies with stellar mass between $\log(M_{\rm star}/{\rm M}_{\odot}) = 10.5$ and 11.

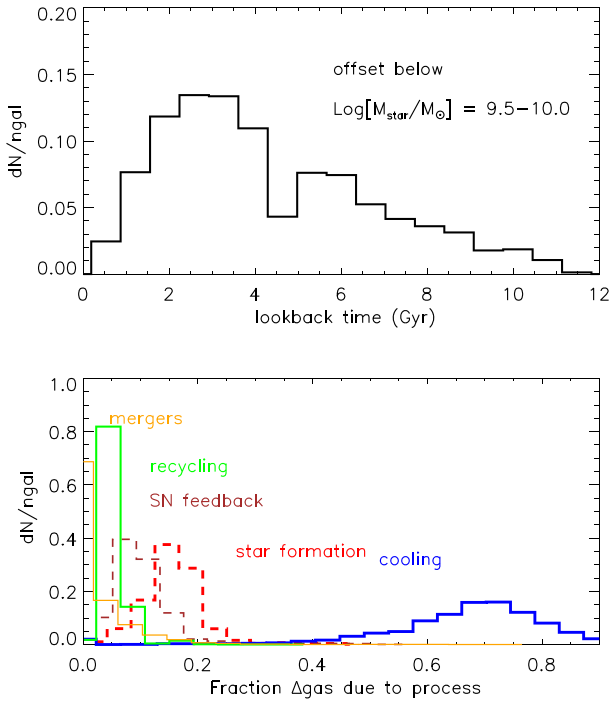

Figure A3. As in Fig. 10, but for galaxies with stellar mass between $\log(M_{\rm star}/{\rm M}_{\odot}) = 9.5$ and 10.

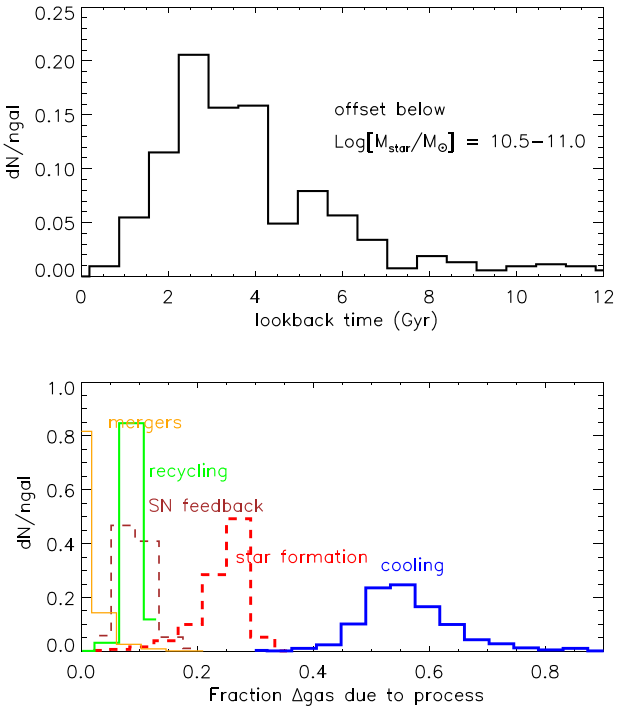

Figure A4. As in Fig. 10, but for galaxies with stellar mass between $\log(M_{\rm star}/{\rm M}_{\odot}) = 10.5$ and 11.

This paper has been typeset from a TEX/LATEX file prepared by the author.